Characterization of the groundwater flow system in the hillside and coastal aquifers of the Mersin-Tarsus region (Turkey)

Zubeyde Hatipoglu · Louis H. Motz · Celal Serdar Bayari

Abstract In the region between Mersin and Tarsus cities, located along the Mediterranean Sea coast in southern Turkey, the demand for groundwater has increased dramatically as the available surface water supplies have already been developed. Fundamental information is required to characterize the existing groundwater system in this area in order to establish a sustainable groundwater-use policy. For this purpose, hydrochemical and environmental isotopic data were collected and integrated with available geological and hydrogeological information to develop a conceptual model of the system. Results, backed up mainly by depleted stable isotope composition and infinitesimal tritium content, suggest that most of the groundwater along the coastal zone is supplied by the neighboring mountain belt while local precipitation has also contributes to aquifer recharge. The validation of the conceptual perspective by a steady-state numerical groundwater flow model reveals that about 90% of the recharge to the aquifer system is supplied by the deep flow of karstic groundwater fed from the Taurus Mountains. Monitoring of changes in the recharge regime of the mountain sector seems to be critical in establishing future groundwater use policies.

Received: 11 March 2008 / Accepted: 3 July 2009
Published online: 25 July 2009

© Springer-Verlag 2009

Z. Hatipoglu (✉)
Department of Geological Engineering, Applied Geology Division,
University of Mersin,
Ciftlikkoy, 33342 Mersin, Turkey
e-mail: zubeyde@mersin.edu.tr
Tel.: +90-324-3610001
Fax: +90-324-3610032

L. H. Motz
Department of Civil and Coastal Engineering,
University of Florida,
Gainesville, FL 32611, USA
e-mail: lmotz@ce.ufl.edu

C. S. Bayari
Department of Geological Engineering,
Hydrogeological Engineering Section,
Hacettepe University,
06532, Ankara, Turkey
e-mail: serdar@hacettepe.edu.tr

Key words Numerical modeling · Radioactive isotopes · Stable isotopes · Karst · Turkey

Introduction

In the presence of water supply, the coastal areas in the temperate climate zones of the world have always been subject to intensifying social and economic activities because of the favorable conditions such as mild climate favoring agricultural production, ease of transportation and settlement. However, sustainable use of groundwater in these areas requires a robust understanding of the hydrogeological system with particular reference to recharge and discharge processes. The literature abounds with cases of severely depleted coastal groundwater resources in areas where water-use policies have not been properly implemented or regulated on the basis of realistic conceptual flow models. These models, which can be built on the basis of reliable field data, should also be tested and improved by use of numerical flow models before serving them to policy makers (e.g. Bayari and Kurttas 2002; Boronina et al. 2003; Idrysy and Smedt 2006; Palma and Bentley 2007; Fetter 2007; Jiao et al. 2008; Vandenbohede et al. 2009).

The region around the cities of Mersin and Tarsus, located on the southern coast of Turkey, has been subject to rapid agricultural and industrial development during the last several decades. This development causes a considerable internal migration from rural areas so that the current regional population of 1,082,000 in 2000 is expected to exceed 2 million by the year 2015 (Governorship of Mersin 2006). Currently, the region is composed of a mixture of residential, agricultural, and industrial areas and seaside resorts. At present, part of the drinking and irrigation water demand is supplied by the Berdan Dam, located to the northeast of the studied region. However, groundwater is also widely used for domestic, agricultural, and industrial purposes, particularly in the coastal part of the study area. Groundwater is preferred to surface water obtained from open canals because of the high suspended solids content of the surface water which blocks irrigation pipes. In addition, groundwater is also increasingly preferred in industrial use because of its annual stability of physical and chemical properties. Moreover, an increasing number of summer resorts, which are situated

 DOI 10.1007/s10040-009-0504-5

mostly along the western coast, almost always meet their potable water demand from groundwater via private wells. While the increasing population and the current socio-economic development trend will obviously increase the pressure over the share of available water resources among domestic, agricultural and industrial use, a reliable assessment of the available groundwater potential has not been made so far. This study aims at a comprehensive assessment of the hydrogeological system because the available geological (e.g. Senol et al. 1998), hydrogeological (e.g. Turkmen 1978), and hydrochemical data (e.g. Demirel 2004) provide only a preliminary insight on the existing aquifers. Accordingly, a conceptual hydrogeological model of the groundwater system has been established based on chemical and isotopic data collected. The conceptual model has been tested by use of a steady-state numerical groundwater flow model (i.e. MODFLOW; McDonalds and Harbaugh 1988; Harbaugh and McDonald 1996) to provide quantitative information on the future groundwater use.

Study area

Location, morphology and climate

The study area encompasses the cities of Mersin and Tarsus and their vicinity along the southern coast of Turkey (Fig. 1). Most of the ~800-km^2-large study area, which is situated between 34°20′N and 34°57′N latitudes and 36° 38′E and 37°00′E longitudes, comprises a large coastal plain that is bounded by the Mediterranean Sea to the south and the flank of the Taurus Mountains to the north. Eight perennial rivers, with a total drainage area of 4,062 km^2, originate from the karstic springs in the mountain sector. These rivers run through the coastal plain to form deltas of various sizes at the coast (Turkmen 1978). Among all, the Berdan River, with its length of 124 km and mean annual discharge of about 39.73 m^3/s is the largest stream in the area. The mean annual discharges of the Delicay and Efrenk rivers are 3.24 and 2.75 m^3/s, respectively (EIEI, unpublished data, 2002). Discharge rates are not available for the other rivers. Drainage and irrigation canal systems are also widespread in the coastal zone.

From a geomorphologic point of view, most of the study area is a low-lying coastal plain that has been formed by depositional processes associated with past and current braided river systems. Part of the coastal plain located to the east has a flood-plain character because of the spring-time overflowing of the Berdan River. Along the northern boundary of the coastal plain, the scarp of the Taurus Mountains exhibits hillside morphology. The elevation in the coastal plain rises steadily from sea level to a few tens of meters at the boundary with the hillside section where the topographic gradient becomes increasingly steeper further inland. The hillside section with its elevation increasing up to several hundreds of meters forms a transition zone toward the mountain belt where peaks exceed 3,500 m.

The study area is dominated by a Mediterranean type climate with hot and dry summers and mild and wet winters. The mean annual precipitation observed at the Mersin and Tarsus meteorological stations are 602.6 mm (between 1930 and 2002) and 586.6 mm (between 1955 and 1996), respectively. The maximum monthly precipitation occurs usually in December and January, while the minimum precipitation is observed during the summer months (i.e., July and August). The mean annual precipitation in the mountain sector is estimated to be around 1,000 mm. Long-term mean annual air temperature in the coastal zone is 18.5°C, and the minimum and maximum temperatures are observed in February (5.2°C) and August (30°C), respectively (DMI, unpublished data, 2002).

Outline of geology

The stratigraphic sequence in the area starts at the bottom with the Karahamzausagi formation, which is composed of limestone, schist and quartz units deposited during the Carboniferous to Permian period (Senol et al. 1998). This formation is overlain tectonically by an ophiolitic mélange that includes Mesozoic aged limestone blocks (Fig. 1). This part of the geologic sequence crops out mainly in the mountainous part of the study area and is covered by Neogene aged Gildirli, Karaisali, Guvenc, Kuzgun and Handere formations that are located at the south. Among the Neogene formations, the Karaisali formation is dominated by limestone whereas the rest is composed of limestone, sandstone, marl, claystone, siltstone and gypsum alternations. Caliche, a secondary calcium carbonate deposition, overlies these formations along the boundary with the Quaternary alluvium that forms the coastal plain. While part of the alluvium that stretches along the mountain flank is characterized by braided stream deposits, flood plain and deltaic deposits dominate particularly in the eastern part of the plain. Dunes are also observed along parts of the sea coast around the river mouths. Karst phenomena are particularly common in the Karahamzausagi formation and are also observed in carbonate horizons of the Neogene units. Because of the lack of deep geophysical and drilling data, direct information on the type of the basement lithologies that lay underneath the coastal plain does not exist. However, regional geologic structure suggests that the platform type carbonate rocks of Karahamzausagi formation and the wedges of ophiolitic rocks that form the Taurus Mountains to the north extend also southward underneath the coastal plain. These carbonate rocks are characterized with well-developed karstic solution conduits. In other parts of the Turkish Mediterranean coast, these units feed large coastal and submarine springs where they are in direct contact with the sea (Bayari 2008; Gunay and Elkhatib 1988).

Outline of hydrogeology

Based on the lithologic properties of the geologic units, the hydrostratigraphic sequence in the study area includes, from bottom to top, a karstic aquifer comprising of Paleozoic and Neogene carbonates, a cemented granular aquifer of Neogene formations, and the uncemented granular aquifer of

 DOI 10.1007/s10040-009-0504-5

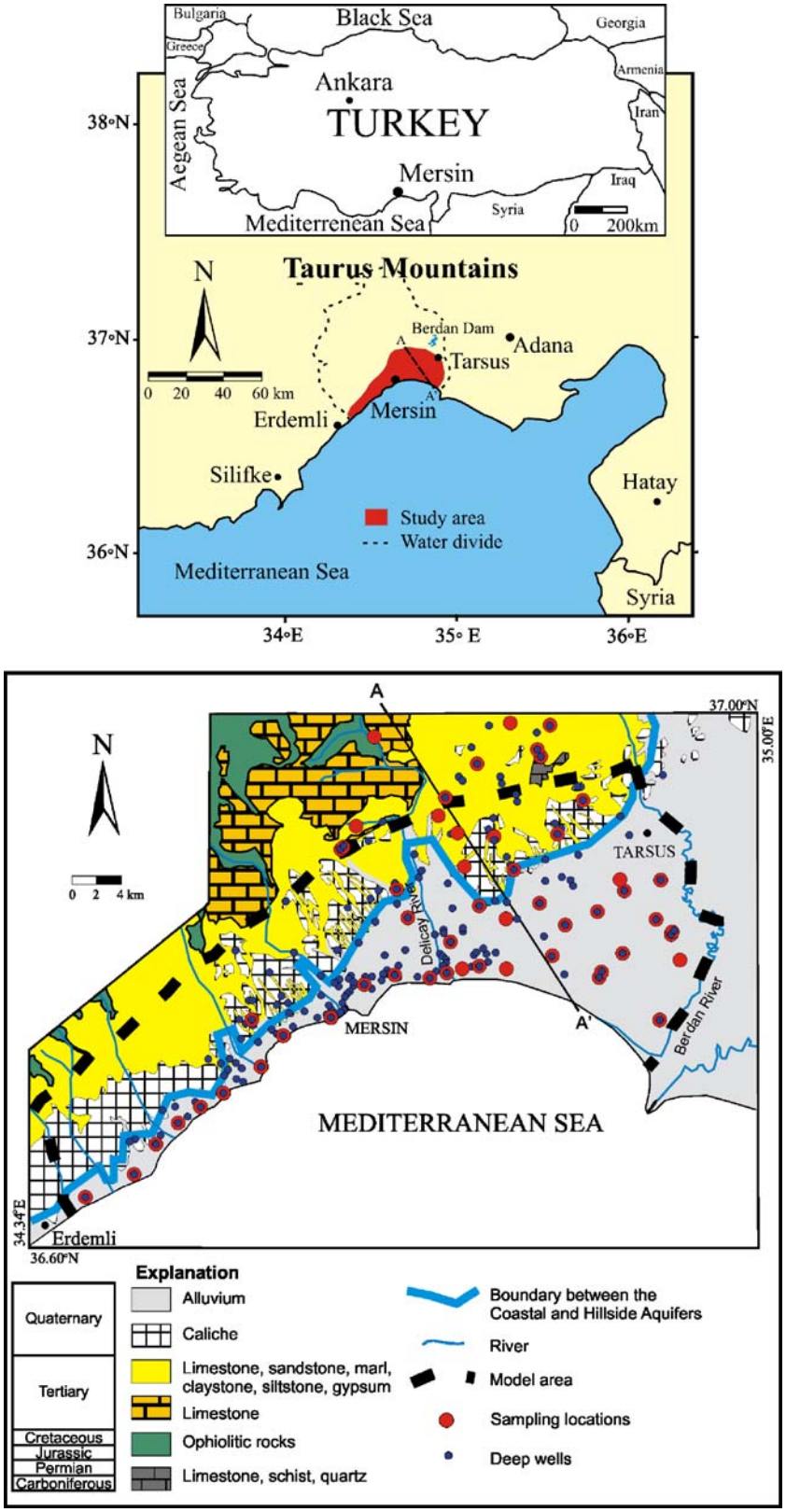

Fig. 1 Location and geologic map of the study area (modified after Senol et al. 1998)

Quaternary units. The Paleozoic karst aquifer, which is characterized by numerous surface karst features (i.e. karrens, solution dolines, uvalas, etc.), covers most of the mountainous area and extends beneath the Hillside Aquifer toward the Mediterranean Sea. The water budget of the deep karst aquifer is practically impossible to establish because of the lack of reliable spatio-temporal information. However, in similar karst settings around the study area, calculations

 DOI 10.1007/s10040-009-0504-5

based on the groundwater's chloride mass balance (e.g. Ozyurt 2005) reveal that such karst aquifers have an effective recharge rate as high as about 70% of the annual precipitation, which is around 1,000 mm/year in this part of the Taurus Mountains. The carbonate rocks belonging to the lower part of the Neogene units possess some degree of karstification as well. According to lithologic logs and pumping test data obtained from deep wells, the Hillside Aquifer, comprising mainly of cemented granular Neogene formations, has a maximum specific discharge of 0.65 l/s/m. On the other hand, the Coastal Aquifer which is made mainly of uncemented Quaternary units has a maximum specific discharge of 21.4 l/s/m (DSI, unpublished data, 2002; KHGM, unpublished data, 2002; Hatipoglu 2004; Fig. 1). The relatively low yield of wells in the Neogene units implies that none of these wells reaches the karstic conduits located at depths. The alluvial deposits of the Coastal Aquifer, which has a surface area increasing considerably from west to east, consist of a heterogeneous mixture of gravel, sand, silt, and clay. In the eastern part of the coastal plain, a clay unit with remarkable areal extent confines the underlying sediments that comprise of more permeable and hydraulically connected coarse-grained material which is separated locally by relatively thin clay layers. The Coastal Aquifer consists of the deeper units in which groundwater occurs under flowing or rising artesian conditions and shallower units where water table conditions dominate. Based on the geologic cross sections (see Fig. 2), the maximum depth of the Coastal Aquifer is estimated to be around 340 m below sea level along the coastline (Hatipoglu 2004). The rivers in the study area are fed mainly by the karst aquifer in the mountainous zone and discharge into the Mediterranean Sea after passing through the coastal plain. The major rivers such as Berdan, Efrenk and Delicay have long-term discharge observations, whereas the minor streams only have momentary data. The mean annual discharge of minor streams has been estimated by comparing the ratio of discharge rate to catchment area size of major rivers to the catchment area size of minor rivers. Accordingly, the mean annual discharge of all rivers was estimated as ~15 m^3/s. Based on long-term data, the base flow through the Hillside and Coastal Aquifers appears to be around 5 m^3/s. Field observations point out that the groundwater discharge from the Hillside and Coastal Aquifers help these rivers to sustain their flow during the dry period.

Methods

To characterize the geochemical processes within the Hillside-Coastal Aquifer system, 53 water samples were collected from springs, and shallow and deep wells during the period between May and June 2003. Standard analytical procedures (e.g. APHA, AWWA, WPCF 1989) were followed in the collection, preservation, and analyses of these samples. Specific electrical conductivity (EC) and temperature were measured in situ using a YSI 33 Model SCT (salinity, conductivity, temperature) Meter; pH was measured with an Orion 290A Model pH Meter and the dissolved oxygen (DO) was measured with a YSI Model 57 DO Meter. Field instruments for EC and pH measurements were calibrated against traceable standard solutions in the laboratory and the DO calibration was carried out in situ against atmospheric pressure. The temperature, EC, DO and pH measurement were accurate within +/– 0.4°C, +/– 5% of measurement, +/– 0.1 mg/l and +/– 0.01 units, respectively.

All water samples were collected from pumping wells after the stability of temperature and electrical conductivity, as an indicator of representative groundwater outflow, was achieved. Because all deep wells have screen at varying depths, the samples had a depth-integrated nature. All samples were collected in double-capped polyethylene bottles, which had been pre-cleaned in the laboratory. Cation samples were kept by adding pure HNO_3 to make pH < 2 and the anion samples were kept cool until analyses, which were carried out within several days. Determination of the major ion composition of water samples was carried out by means of standard methods. Cations (i.e. Ca, Mg, Na, and K) were measured with a

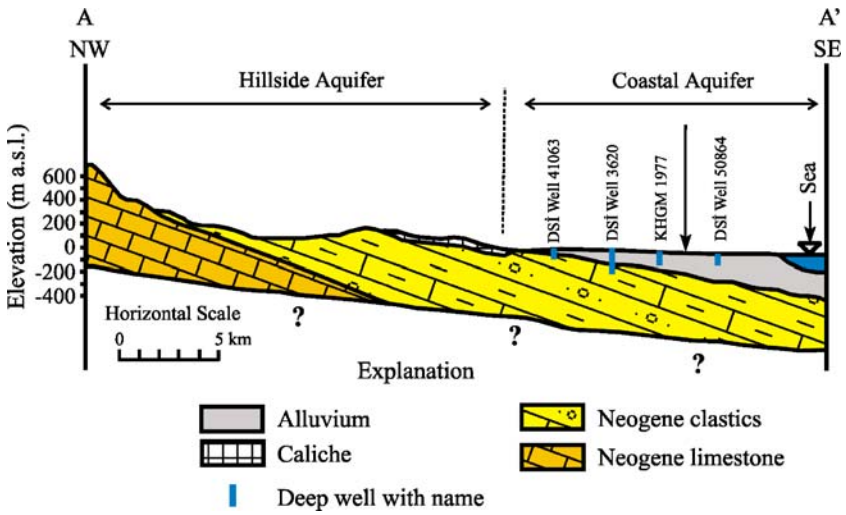

Fig. 2 Extent of geologic units across *A–A′* cross-section

 DOI 10.1007/s10040-009-0504-5

Perkin Elmer Model 2280 atomic absorption spectrophotometer, SO_4 was measured with a Bausch-Lomb Model Spectronic 21 spectrophotometer and the rest of the anions (i.e., Cl, HCO_3 and CO_3) were measured by titrimetric procedures. All samples had ionic balance errors less than +/– 5% and their total anion or cation contents are in agreement with the field-measured EC data. Results of physical and chemical characteristics of groundwater samples, as well as the main characteristics of sampling sites, are presented in Table 1.

To estimate the recharge area elevation and the residence time, 28 groundwater samples for isotopic analyses (i.e. tritium, oxygen-18 and deuterium) were collected in double-capped polyethylene bottles from springs, and deep and shallow wells during the period May through June 2003. During the collection of isotope samples, special care was given to prevent air bubble inclusion in bottles. Samples for isotopic analyses were kept cool until analyses. The stable isotopic composition of samples was determined with dual-inlet isotope ratio mass-spectrometry by following the standard measurement protocols (i.e. gas equilibrium) in a commercial laboratory. The results are reported in del notation against V-SMOW (Vienna-Standard Mean Ocean Water) reference standard. Analytical uncertainty for ^{18}O and ^{2}H measurements are in the order of 0.1‰ V-SMOW and 1‰ V-SMOW, respectively. Tritium (^{3}H) compositions were determined by means of liquid scintillation counting after alkaline electrolytic enrichment at the Hacettepe University. An IAEA (International Atomic Energy Agency) dead water blank and NIST SRM 4927F standard were used in tritium analyses. Results are reported in TU (Tritium Unit) and have an analytical uncertainty ranging from +/– 0.2 TU to +/– 0.4 TU (1 sigma error). Results of isotopic analyses are presented in Table 2 along with respective site information.

A conceptual model of the aquifer system was developed based on the interpretation of available chemical and isotopic data and it has been tested by using a numerical flow model. For this purpose, a three-dimensional finite-difference groundwater flow model (MODFLOW; McDonalds and Harbaugh 1988; Harbaugh and McDonald 1996) with Processing MODFLOW processor, PMWIN (Chiang and Kinzelbach 2001) was used to simulate the aquifer system. The model was applied in the PMWIN environment and run as a steady-state simulation to represent the groundwater system in the period 2000–2001 for which a reasonable observed head distribution was available. The absence of historical head and pumping data did not allow for transient modeling.

Results

Hydrochemistry

Hydrochemical data (see Table 1) provide important clues on the physical and chemical processes operating in the groundwater flow system of the study area. In a pristine, homogenous and isotropic coastal groundwater flow system where the flow is driven by gravitation from a mountain range toward the sea, the temperature and EC are expected to increase towards the sea boundary due to geothermal heat flux and continuing water–rock interaction. Similarly, the DO is expected to decrease due to oxidation reactions that prevail along the flow routes. The behavior of pH would depend on the carbon dioxide source (i.e. open or closed) and the type of water–rock interaction throughout the flow system. A preliminary review of the field-measured parameters (i.e. temperature, pH, DO and EC) reveals a complex spatial distribution pattern (Figs. 3 and 4) which seems to be governed by the interaction of many factors such as geothermal gradient, atmospheric heat flux from surface, residence time, hydraulic and geochemical properties of flow medium and seawater intrusion etc. Despite these complicating factors, spatial distribution of field-measured parameters appear to be linked with the site′s depth of sampling so that shallow and deep flow systems have slightly different parameter values. However, similar parameter values (e.g. temperature) are also observed both in the shallow and deep flow systems probably because of the processes that operate locally (e.g. local heat flux). The deep flow system (marked by A in Fig. 3) is characterized by the wells that are deeper roughly than 100 m and extends mostly along the coastal plain as well as two other sites (e.g. 151, 152, 169 and 170) located further inland. This flow system comprises of cool (< 30 C) and hot components (sites 169, 170), which have remarkably different temperature and EC values (see Fig. 3). Many of the deep wells (up to 300 m) are clustered in the eastern part of the coastal plain where local vertical recharge to the deep flow system is restricted by a vast clay cover. Surprisingly, the groundwater in this particular region is characterized by low temperature (20–24 C), low EC (385–960 μS/cm) and relatively low DO (2.4–5.8 mg/l) values which is not expected from a deep flow system that should be subject to more geothermal heat flux. As indicated by the isotope data (see below) the deep groundwater in this area is fed mainly by the deep karstic conduits that extend toward the Taurus Mountains. While low temperature and EC are not usual for a deep flow system, it is probably the fast flow of karst groundwater that keeps the geothermal heat flux and water–rock interactions at limited level. Unfortunately, none of the deep wells has temperature and/or electrical conductivity profile data that can shed light on the status of deep and shallow flow systems in the study area.

The shallow flow system comprising mostly of springs and wells that are less than 100 m deep (sector B in Figs. 3 and 4) is characterized by cool groundwater with a wide range of temperature (20–28 C), EC (450–1,700 μS/cm) and DO (2.2–9.2 mg/l) values. In general, the shallow groundwater gets warmer around the coastal zone probably because of the atmospheric heat flux that becomes more effective as the water table elevates to ground surface. The large scattering in EC values in the shallow flow system is probably linked with the evaporite minerals that are dispersed in the Neogene and Quaternary units. Similarly, the wide range of DO values implies that the

 DOI 10.1007/s10040-009-0504-5

Table 1 Physical and chemical characteristics of groundwater samples

Sample site number	Sampling date (2003)	Coordinates		T (°C)	pH	EC (μS/cm)	DO mg/l	Concentration (meq/l)								Well depth (m)
		X	Y					Na	K	Ca	Mg	CO_3	HCO_3	Cl	SO_4	
120	19.05	670393	4083006	23	7.34	550	NA	0.74	0.09	2.72	2.60	0	4.87	0.84	0.78	68
122	19.05	671564	4078742	24	8.01	385	2.5	2.11	0.25	1.04	1.32	0	3.35	0.85	0.16	300
123	19.05	672049	4076853	21	7.66	700	3.8	4.95	0.09	1.21	2.25	0	5.28	1.45	1.46	~10
124	19.05	667294	4077441	21	7.36	850	4.4	4.31	0.08	3.08	3.12	0	4.77	3.24	1.68	117
125-A	19.05	665471	4075398	24	7.75	1,250	4.2	7.17	0.08	2.81	4.05	0	5.28	4.73	3.43	50
125-B	19.05	665470	4075391	23	7.7	950	2.4	5.22	0.04	2.04	2.84	0	4.21	3.20	2.43	120
126	19.05	670399	4072109	22	7.97	700	2.4	3.41	0.08	1.76	2.22	0	4.37	1.85	1.03	249.8
128	19.05	670126	4080277	21	7.47	500	4.1	1.21	0.06	3.65	2.56	0	5.89	0.41	0.52	25
129	19.05	667434	4082695	22	7.55	600	4.1	1.32	0.17	4.13	1.86	0	4.97	0.94	0.97	24
130	19.05	667081	4083642	20	7.2	500	3.2	0.89	0.11	4.21	1.88	0	5.18	0.51	0.85	Spring
131	20.05	665189	4080917	21	7.57	842	5.8	1.60	0.10	4.54	2.79	0	6.40	1.05	0.75	~100
132	20.05	661900	4087345	24	7.7	1,061	6	5.06	0.34	1.90	3.84	0	6.50	1.49	2.18	~100
133	20.05	660319	4081589	25	7.19	960	3.9	2.39	0.07	3.81	4.17	0	8.98	0.68	0.64	140
134	20.05	662497	4079822	21	7.67	831	2.4	3.88	0.13	1.29	3.17	0	5.63	1.25	1.30	~100
135	20.05	661472	4077216	24	7.67	826	2.6	3.60	0.13	1.67	3.01	0	5.28	2.12	1.01	106
136	20.05	655052	4081403	23	8.06	1,400	3.6	12.10	0.30	1.13	2.29	0	7.82	4.29	2.57	106
137	20.05	657562	4080316	23	7.29	950	4.8	2.49	0.10	4.33	4.56	0	8.02	1.61	1.01	16
138	20.05	657577	4076153	26	7.9	800	3	4.06	0.10	1.27	3.23	0	4.57	2.52	1.18	~10
139	20.05	655305	4076339	25	7.45	1,300	2.8	2.47	0.17	4.72	8.94	0	8.38	2.23	4.71	30
140	20.05	653885	4076105	21	7.36	880	4.6	1.21	0.06	3.37	6.12	0	7.87	1.09	1.19	~10
141	20.05	652629	4075739	22	7.59	600	5.8	0.69	0.08	3.03	4.52	0	7.21	0.54	0.77	36
142	20.05	651342	4075115	21	7.44	800	4.2	1.37	0.07	3.61	5.51	0	8.12	1.01	0.91	15
143	21.05	663958	4090200	22	7.59	730	7.2	1.20	0.11	5.26	2.40	0	7.16	0.90	0.86	~100
144	21.05	660206	4094377	24	7.37	900	5.8	2.61	0.28	6.46	2.36	0	8.68	1.15	1.87	80
145	21.05	657898	4096609	20	7.1	1,150	2.2	1.74	0.07	9.68	3.44	0	7.82	2.48	4.64	~10
146	21.05	660465	4093770	21	7.05	1,000	6.1	2.24	0.08	8.22	1.77	0	8.12	1.07	2.98	80
147	21.05	661238	4096347	26	7.28	1,100	NA	1.62	0.10	8.98	1.85	0	9.29	1.70	1.43	48
148	21.05	658231	4084393	24	7.34	980	5.6	1.63	0.12	5.38	4.82	0	8.17	1.83	1.18	82
149	21.05	656608	4086855	NA	7.82	950	6.1	22.63	0.35	1.90	5.72	0	8.98	7.31	13.27	130
150	21.05	655186	4093202	25	7.31	930	5.6	1.92	0.16	6.59	1.66	0	7.97	0.87	2.54	~100
151	21.05	651966	4088827	23	6.82	1,300	3.2	3.17	0.13	11.95	5.84	0	6.45	2.02	10.92	Spring
152	21.05	652430	4090424	24	7.38	700	5.2	1.42	0.08	5.18	1.18	0	5.69	0.87	0.82	100
153	21.05	645987	4094893	20	7.51	450	9.2	0.48	0.04	4.45	1.12	0	5.33	0.24	0.44	Spring
154	21.05	642932	4072062	23	7.74	1,700	6.2	11.46	0.08	3.74	6.01	0	8.53	10.47	1.92	74
155	21.05	638996	4070259	25	7.55	1,280	5.2	4.60	0.09	5.43	3.16	0	8.58	2.52	1.38	35
156	22.05	636372	4071875	27	7.88	700	4	2.61	0.12	2.81	1.67	0	5.69	0.62	0.57	150
157	22.05	626681	4058734	24	7.37	750	5.6	0.84	0.05	5.50	2.97	0	7.41	0.72	0.57	100
158	22.05	622620	4056910	23	7.72	550	5.2	1.22	0.06	2.24	2.52	0	5.08	0.55	0.38	35
159	22.05	628999	4061184	28	7.73	1,380	5.6	5.75	0.21	4.02	5.04	0	7.92	5.03	1.26	80
160	22.05	630879	4063203	24	7.61	810	6.3	1.92	0.07	4.00	3.13	0	7.11	0.83	0.80	~100
161	22.05	632320	4064510	24	7.51	850	6.6	1.91	0.09	5.00	2.70	0	7.31	0.86	0.77	100
162	22.05	634197	4065577	21	7.12	700	5.8	1.32	0.10	5.26	1.77	0	6.60	0.63	1.08	~100
163	22.05	637847	4067892	25	7.55	1,300	4.2	4.58	0.15	3.77	6.47	0	8.53	4.16	1.19	16
164	23.05	652920	4078390	23	7.79	580	5.4	0.78	0.06	2.40	3.40	0	6.50	0.38	0.46	50
165	23.05	654114	4084627	22	7.36	720	5.6	1.07	0.09	3.87	2.70	0	6.50	0.94	0.58	23
166	23.05	653487	4087463	23	7.47	1,700	5.5	5.72	0.30	5.80	8.34	0	10.66	6.24	2.09	~10
167	23.05	648422	4082760	22	7.49	850	2.6	2.17	0.02	5.68	2.17	0	7.06	0.61	1.55	35
168	23.05	645078	4088081	20	7.38	550	5.1	0.29	0.02	5.32	0.72	0	5.89	0.25	0.14	Spring
169	23.05	644083	4086158	40	7.59	10,900	1	93.31	2.00	8.71	4.51	0	3.05	105.23	8.50	220
170	23.05	643921	4086202	38	7.59	11,000	1.1	96.60	2.24	9.55	4.80	0	3.05	103.69	8.34	~100
171	23.05	649367	4080305	21	7.61	1,030	4	3.96	0.08	4.23	2.61	0	7.61	0.74	1.80	29.5
172	23.05	648320	4075640	26	7.9	950	5.8	2.44	0.06	5.06	2.66	0	7.11	2.36	0.62	132
174	23.05	645749	4074848	23	6.79	1,000	6.1	2.15	0.05	5.70	4.73	0	7.92	2.36	1.48	73

NA not available

DOI 10.1007/s10040-009-0504-5

Table 2 Groundwater's isotopic composition

Sample site number	Coordinates		Sampling date (2003)	^{2}H (‰ V-SMOW)	^{18o} (‰ V-SMOW)	^{3}H (TU)	Well depth (m)
	X (UTM, 36 N)	Y					
120	670393	4083006	19.05	–53	–10.2	6.57	68
123	672049	4076853	19.05	–54	–10.1	0.36	~10
125-a	665471	4075398	19.05	–37	–7.4	0	50
125-b	665470	4075391	19.05	–44	–8.8	0	120
126	670399	4072109	19.05	–53	–12.0	0	249.8
128	670126	4080277	19.05	–53	–10.3	2.18	25
142	651342	4075115	20.05	–42	–8.4	5.28	15
143	663958	4090200	21.05	–35	–7.6	4.09	~100
144	660206	4094377	21.05	–34	–7.0	3.77	80
156	636372	4071875	22.05	–35	–6.1	0	150
157	626681	4058734	22.05	–45	–7.7	3.66	100
162	634197	4065577	22.05	–41	–7.5	6.08	~100
167	648422	4082760	23.05	–46	–7.6	5.17	35
168	645078	4088081	23.05	–43	–7.6	2.30	Spring
169	644083	4086158	23.05	–67	–10.3	0	220
171	649367	4080305	23.05	–45	–7.6	5.64	29.5
172	648320	4075640	23.05	–35	–5.9	0.78	132
122-a	671563	407874	22.06	–59	–9.3	1.23	87.6
122-b	671564	4078742	22.06	–54	–9.6	0	300
148	658231	4084393	22.06	–34	–6.7	3.11	82
149	656608	4086855	22.06	–38	–7.0	5.58	130
135	661472	4077216	22.06	–49	–8.6	0.10	106
134	662497	4079822	22.06	–43	–7.7	0.24	~100
133	660858	4080766	22.06	–49	–8.7	2.47	~10
166	653487	4087463	23.06	–32	–6.2	4.21	~10
151	651966	4088827	23.06	–35	–6.1	0	Spring
153	645987	4094893	23.06	–42	–7.3	4.32	Spring
152	652430	4090424	23.06	–37	–6.9	0.59	100

rate of redox reactions varies considerably at different parts of the shallow system. In fact, this is an expected situation in a coastal aquifer which contains abundant organic matter in low and high velocity flow zones. Among all field-measured parameters, the distribution of pH does not reveal any information specific to shallow or deep flow systems. Remarkably low pH values observed in several spots (e.g. sites 151 and 174) may also be associated with mantle and/or crustal carbon dioxide flux but available data are far from supporting this argument.

Based on the major ion distribution, three different hydrochemical facies types can be defined: (1) a fresh groundwater zone of Ca/Mg–HCO_3 facies, (2) seawater intrusion zone of Na–Cl facies and (3) a transitional Na–HCO_3 facies in which previously saline groundwater is being flushed by Ca/Mg–HCO_3 type water (Fig. 5). Type 1 groundwater, represented by Ca–HCO_3 facies, is prevalent in most of the study area and suggests a groundwater composition that is typical of carbonate aquifers. Dominance of the Mg cation in some of these samples is attributed to contact of groundwater with ophiolitic rocks, which are common at the mountain flank (Hatipoglu and Bayari 2005b). Type 2 groundwaters belonging to NaCl facies are represented by two thermal groundwater wells located inland (i.e. sites 169 and 170) and a coastal well (i.e. site 154) from which cool groundwater has apparently been over pumped. While the Na–Cl facies observed in the inland wells implies presence of a deep fault system that probably extends down to the freshwater/salt-water interface, the stable isotope composition in one of these wells suggests limited seawater contribution (see below). The origin of salinity in these wells appears to be associated with the dissolution of evaporite minerals (e.g. Halite, NaCl). On the other hand, the limited extent of NaCl facies along the coastal zone where groundwater abstraction for domestic use is common suggests a strong groundwater outflow to the sea. Type 3 waters of Na–HCO_3 facies spread mainly in the southeastern part of the study area and indicate an aquifer zone that has been previously affected by seawater intrusion but now is being flushed by fresh groundwater (Appelo and Postma 2005). Because the thick clay cover does not allow for effective groundwater recharge from surface in this area, the ongoing flushing process appears to be maintained by the deep groundwater flow, which is fed from the Taurus Mountains. The groundwater system in the study area also includes Na–SO_4 and Ca–SO_4 type of groundwaters as isolations in the north. These waters are probably associated with evaporate deposits which are dispersed sparsely in the Neogene and Quaternary units.

Environmental isotopes

Environmental isotope data of selected groundwater samples (see Table 2) provide a more robust insight in recognition of the deep and shallow flow systems in the study area. The stable isotopic composition of precipitation as the prime source of groundwater is spatio-temporally variable and has been observed globally by the IAEA at a number of stations. Fortunately, one of these stations (i.e. Adana, IAEA ID No. 1735000), is located 30 km to the east of the study area at 73 meters above sea level (m asl) and has a long record of isotope data of the local precipitation. The long-term (i.e. between

 DOI 10.1007/s10040-009-0504-5

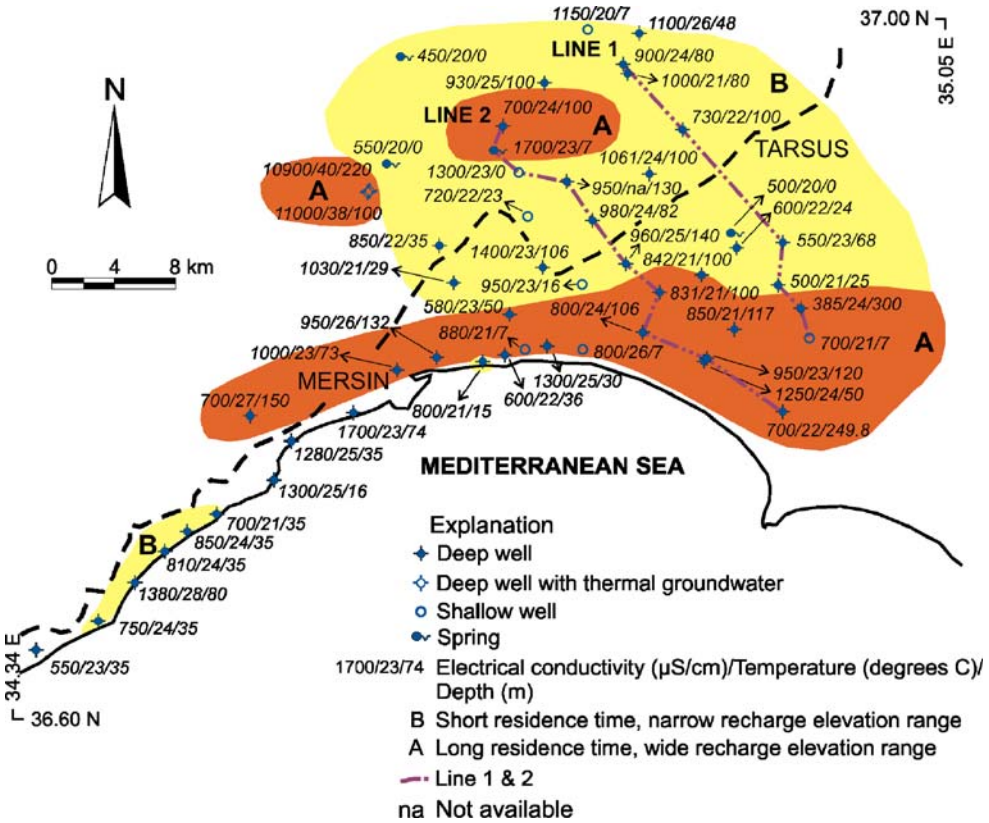

Fig. 3 Spatial distribution of EC, temperature and depth of sampling

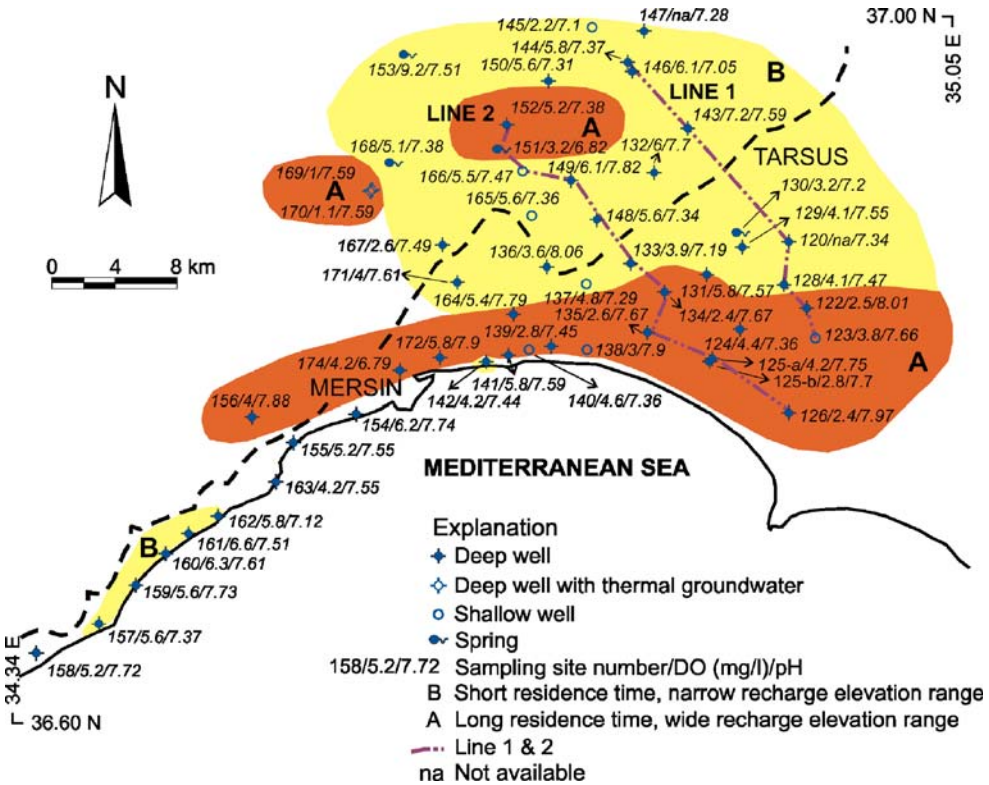

Fig. 4 Spatial distribution of sampling sites (number), DO and pH

 DOI 10.1007/s10040-009-0504-5

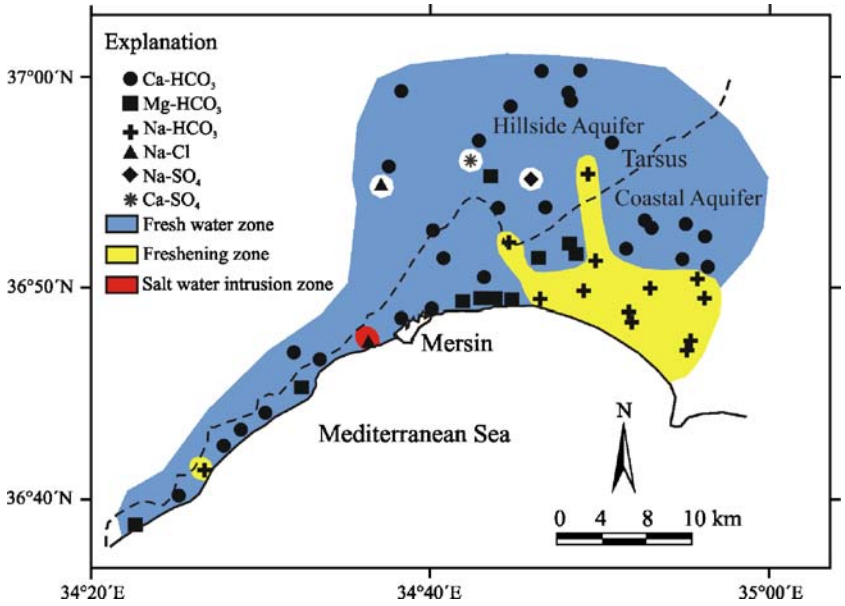

Fig. 5 Hydrochemical facies distribution in the study area

1963 and 1987) mean annual precipitation weighted ^{18}O and ^{2}H compositions observed at this station are –5.5‰ V-SMOW (+/– 0.74, 1 sigma) and –28.0‰ V-SMOW (+/– 4.8, 1 sigma), respectively (IAEA 1992). The extreme stable isotope compositions during the same period range between –3.91 and –7.68‰ V-SMOW for ^{18}O and between –17.3 and –35.5‰ V-SMOW for ^{2}H. The precipitation weighted ^{3}H composition at this station was about 10 TU in the early 1990 s and currently is around 5 TU. Previous studies carried out in parts of the Taurus Mountains close to the study area reveal that the stable isotopic composition of precipitation becomes depleted as the elevation of precipitation increases toward mountain peaks (Ozyurt and Bayari 2007). Long-term mean values for ^{18}O and ^{2}H at around 2,100 m asl in the Aladaglar Basin (> 3,700 m) located 80 km to NNE of the study area are reported to be –10.7 and –70.0‰ V-SMOW, respectively (Ozyurt 2005).

The stable isotope composition of the groundwater samples clusters around the Eastern Mediterranean Meteoric Water Line (EMMWL, Fig. 6) which has a deuterium excess value (i.e. $\delta^2H = 8 \times \delta^{18}O + 22$; Gat and Carmi 1970) greater than that of the Global Meteoric Water Line (i.e. +10; Craig 1961). In fact, this is an expected situation because most of the precipitation around the study area is known to be fed by the air moisture of the Eastern Mediterranean region (Bayari 1991). On the other hand, almost all of the groundwater samples have stable isotope compositions that are more depleted than the long-term mean of the stable isotope composition observed at the Adana station. This suggests that most of the recharge to the groundwater system in the study area is supplied by precipitation that occurs at elevations higher than the coastal plain. In this regard, the magnitude of depletion in stable isotope composition compared to Adana precipitation is fairly striking. The most depleted samples possess ^{18}O and ^{2}H contents as low as –12 and –70‰ V-SMOW, respectively. These values imply a recharge area elevation of around 2,000 m, if it is assumed that the stable isotope vs. elevation relationship defined for the Aladaglar Basin is also valid for this part of the Taurus Mountains. The most isotopically depleted samples belong to the eastern

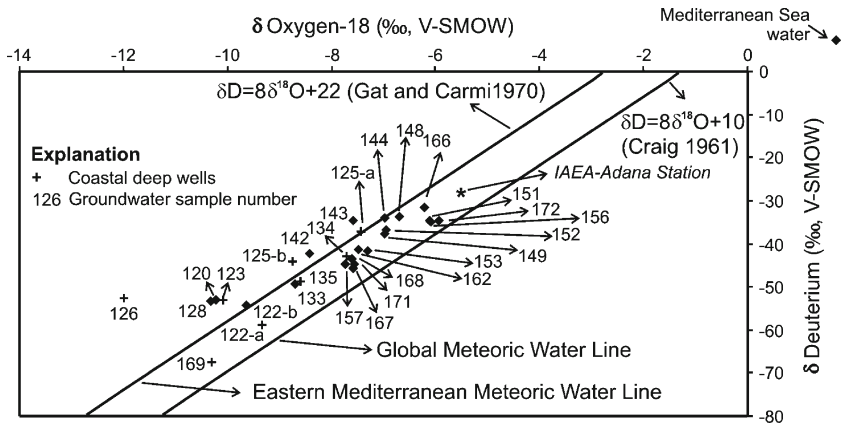

Fig. 6 Scatter plot of stable isotope composition

 DOI 10.1007/s10040-009-0504-5

coastal plain so that the degree of depletion increases toward the coastline probably because the deep flow lines fed by higher altitudes converge along the freshwater/seawater interface (Fig. 7). The samples belonging to the downstream part of the eastern coastal plain, where vertical recharge to the aquifer is prevented by the surface clay layer, have the most depleted stable isotopic composition (see lines 1 and 2 in Fig. 7). This indicates that the stable isotope signal of high altitude precipitation is preserved well if it is not mixed with local recharge (or shallow groundwater) which is characterized by relatively more enriched stable isotope composition.

The stable isotopic composition of seawater around the study area is characterized by ^{18}O and ^{2}H values of +2 and +10‰ V-SMOW, respectively (Bayari 2008). In this context, the stable isotopic composition of the groundwater samples does not indicate an accountable shift from the EMMWL to the seawater so that the mixing between fresh groundwater and seawater is negligible. This observation is in agreement with the deductions based on chemical composition (e.g. EC values) that indicate negligible mixing, if it exists at all. Even the thermal groundwater sample with the most elevated EC value at site 169 (see Fig. 6) does not suggest an accountable contribution from seawater so that its chemical composition (NaCl facies) should most probably be a result of the dissolution of halite that exists within the localized evaporite deposits of the Neogene formations.

Currently, the precipitation weighted mean annual tritium content of the Adana station is around 5 TU, whereas the monthly values usually scatter at +/– 2 TU around this value. The tritium content is a direct indicator of the groundwater's residence time and decreases with the increasing length of flow. Therefore, the groundwaters with high tritium content are regarded as fed by relatively recent precipitation that moves through short/shallow flow paths. Contrarily, the long and/or deep flow paths are expected to carry groundwaters with low or negligible tritium content. A combined analysis of tritium and stable isotope contents (e.g. ^{18}O) of the groundwater samples in the study area reveals a portrait that is in line with above arguments. Almost all of the samples belonging to deep wells scattered mostly in the coastal zone are characterized by tritium contents below detection limit (i.e.0 +/– 0.2 TU). The stable isotopic composition (e.g. ^{18}O) of these samples has a wide range between –4 and –12‰ V-SMOW (Figs. 7 and 8). These suggest that the groundwaters fed both at low and high altitudes may have long residence times. While groundwaters fed at high altitudes are expected to have long residence times (i.e. low tritium content), those fed at lower elevations are normally expected to have measurable tritium content, as they are closer to their recharge area. The samples of eastern coastal plain, characterized by their low temperature, low EC, highly depleted stable isotope composition and tritium contents below or near detection limit, appear to be fed by deep karstic conduits that extend toward the heights of the Taurus Mountains. Furthermore, several isolated groundwater samples in the Hillside Aquifer also possess tritium contents below detection limit, whereas their stable isotope composition indicate recharge from either local (e.g. samples 151, 152) or slightly higher elevations (e.g. samples 169, 170). These observations reveal that while many of the groundwater samples with

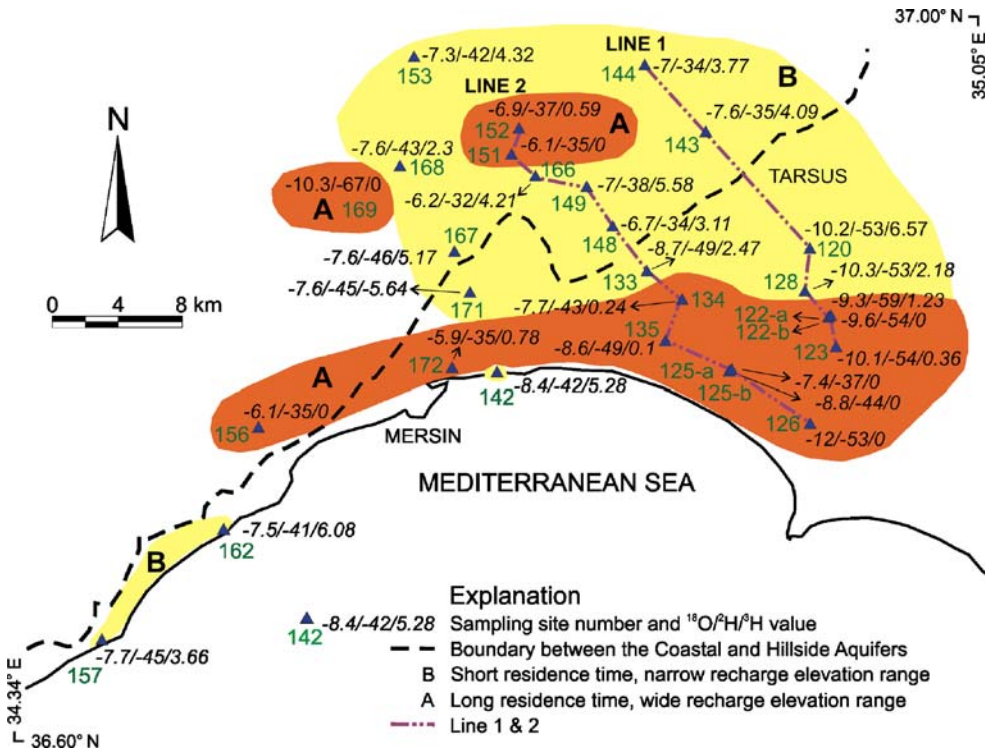

Fig. 7 Spatial distribution of isotopic composition in the study area

 DOI 10.1007/s10040-009-0504-5

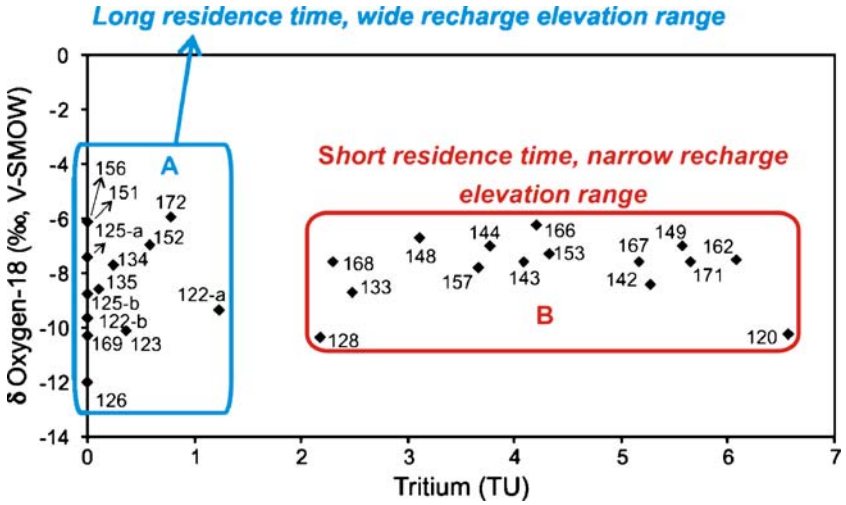

Fig. 8 Relationship between the oxygen-18 and tritium contents of groundwater samples

long residence times in the coastal zone are fed from high elevations, some of those located in the hillside area are fed locally or from moderate elevations. A discrimination based on tritium content reveals that groundwaters with tritium contents above 1.5 TU (e.g. between 2 and 7 TU) have a narrow stable isotope (i.e. ^{18}O) content range compared to those with lower tritium contents. Almost all of these samples belong to the Hillside Aquifer or to the western part of the Coastal Aquifer where it forms a narrow band along the coast. Their isotopic composition reveals a shallow flow system with short residence time (see Fig. 8).

The highest ^{3}H contents observed elsewhere in the study area are within the annual variation range of ^{3}H in current precipitation (i.e. 5 TU +/– 2 TU). Therefore, if piston flow conditions are assumed in the flow domain, the mean half life of ^{3}H (i.e. 12.32 years; Unterwerger and Lucas 2000) reveals mean residence times of 0, 12, 25, 37, 49 and 62 years for the groundwaters that have ^{3}H contents around 5, 2.5, 1.3, 0.6, 0.3 and 0.15 TU, respectively. Considering a plausible analytical uncertainty level of +/– 0.2 TU, the samples with no measurable ^{3}H content should have mean residence times much longer than 60 years.

Conceptual model

The evaluations presented above suggest an aquifer system that includes a complex combination of deep and shallow flow systems (Fig. 9). The deep flow system which dominates particularly in the eastern coastal plain comprises mainly of cool groundwaters that are characterized by a relatively low range of temperature and EC as well as depleted stable isotope composition and tritium contents which are below detection limit. It appears that the presence of a vast clay cover extending in this region causes the deep cool groundwater flow to keep its initial chemical and isotopic signal because of limited contribution from local precipitation. While there is no direct information from local deep karst groundwater, the isotopic and chemical character of groundwater representing the deep cool groundwater flow in the eastern coastal plain resembles very much of the data obtained from karst groundwater in the heights of the Taurus Mountains (i.e. ^{18}O=–13‰ V-SMOW and ^{2}H=–80‰ V-SMOW ; EC=500 μS/cm; Ozyurt 2005). Therefore, the karstic carbonates extending from the Taurus Mountains toward the Mediterranean Sea underneath the Hillside Aquifer appear to be an important supply of the deep cool groundwater in the study area. The two deep inland wells (i.e. sites 169 and 170) with elevated temperature and EC, partially depleted stable isotope composition and below detection limit tritium contents are regarded to be representative of a spatially isolated process that is not influential in the rest of deep groundwater flow system. Similarly, the groundwaters belonging to $CaSO_4$ and $NaSO_4$ facies are also regarded to be local processes that are caused by the dissolution of evaporite minerals scattered in Neogene and Quaternary formations. The shallow groundwater flow is characterized also by a wide range of temperature and EC distribution. However, the samples belonging to this flow system possess a relatively narrow range of stable isotope composition and tritium contents which are greater than 1.5 TU. This shows that shallow flow is sustained by local recharge and has a short residence time. While the study area has a long coastline, the stable isotope composition implies that the seawater intrusion is a negligible process except at a single spot (i.e. site 154). Despite the common groundwater use, particularly in the coastal plain, the negligible magnitude of seawater intrusion indicates a strong recharge from the Taurus Mountains that flow through the aquifer system (see Fig. 1). Eventually, the conceptual flow model of the study area comprises of Hillside and Coastal Aquifers that have different recharge systems. While the Hillside Aquifer is fed partly by local recharge and mostly by recharge from the Paleozoic karst aquifer, a great portion of the recharge to the Coastal Aquifer appears to be provided from the Paleozoic karst aquifer, which is fed from the heights of the Taurus Mountains.

 DOI 10.1007/s10040-009-0504-5

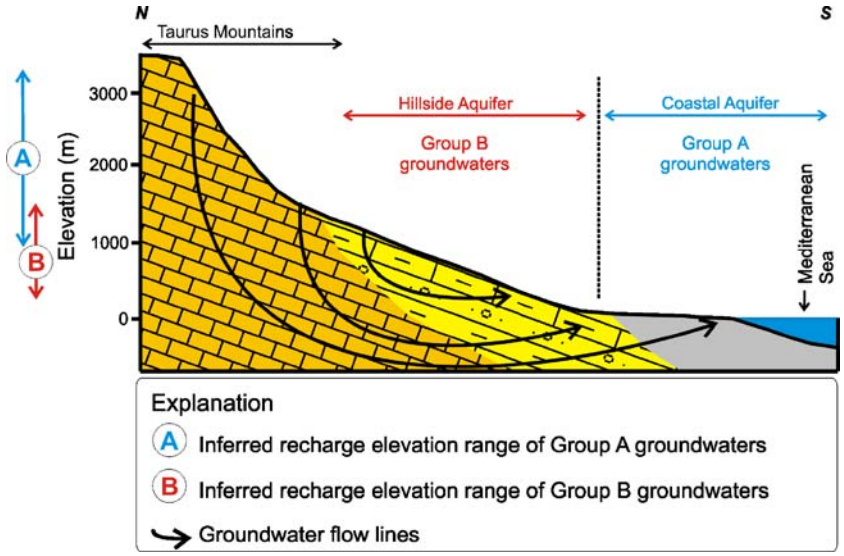

Fig. 9 Sketch showing the conceptual model of regional groundwater flow system

Numerical model

Input data

The groundwater system in the study area was modeled as a single flow domain that comprises of two interconnected aquifers (i.e. the more productive Coastal Aquifer and the less productive Hillside Aquifer). In spite of the complex lithologic structure of these aquifers, they can be considered as a single hydraulically connected system because of the smooth distribution of the water levels with depth. The model area is bounded by the Mediterranean Sea at the south, whereas the northern limit passes roughly through the boundary between the Neogene and older units. The western boundary was arbitrarily chosen to be the location where the Coastal Aquifer reaches a negligible areal extent and the Berdan River formed the eastern boundary. Within the model domain, the elevation of the top of the Coastal and Hillside Aquifers range from 0–40 m and 25–600 m, respectively. The bottom topography of the Coastal Aquifer was determined from the geologic cross sections so that the thickness of the Coastal Aquifer increases from the northern boundary of coastal plain to the sea coast where it reaches a depth of 340 m below sea level.

The effective recharge to model domain is supplied by two sources. Toward the north, the geological and topographic structure of the Taurus Mountains facilitates the collection of a large quantity of water from precipitation which is estimated to be more than 1,000 mm/year (Hatipoglu 2004). Under the influence of gravity, precipitation percolates from the Taurus Mountains to the Hillside and Coastal Aquifers. The flow model accounts for this source by using a specified head boundary along its northern limit. The recharge over the model domain was accounted for by the net precipitation, which is the difference between the measured precipitation minus evapotranspiration (ETP). The measured rainfall during the modeling period at Mersin station was 356 mm/year (DMI, unpublished data, 2002). The ETP losses which were determined both by the Turc (1954) and the Penman-Monteith (Monteith 1965) methods revealed an annual effective recharge rate of 16 and 33 mm/year, respectively. The effective recharge based on the Penman-Monteith method was preferred in the modeling because of its monthly time resolution. As it is not practiced, artificial recharge was not considered in the flow model.

In the study area, spatial groundwater level changes have not been observed systematically. Therefore, the groundwater levels required by the model as observed head distribution throughout the aquifer system were measured at 111 wells during the period between July 2001 and November 2001. The groundwater head data have been collected in a manner that the effect of pumping and recent precipitation input on local groundwater level would be as limited as possible. Because many of the wells where the groundwater head was observed have been in use at different times of the dry period (i.e. summer), a measurement scheme expanding in a wide time interval has to be employed. Head measurements have been carried out at times when each of the wells has not been used for several weeks so that the depression cone could have recovered to a position that represents the local groundwater level in the respective parts of the aquifer. Consequently, many of the head measurements (~76%) have been carried out during the period between 1 September and 10 November. The groundwater level in the rest of the wells has been measured at different times between July and August when they have not been pumped at least for several weeks. During the period of groundwater level measurements, the bulk precipitation corresponded to 17% of mean annual input so that its net effect on groundwater level is assumed negligible because of the extreme evapotranspiration during the summer. The groundwater levels ranged from 1 m below sea level to 385 m above sea level and the typical depths to groundwater surface from land surface were between 2 m and 5 m for the Coastal Aquifer and between 3 and 11 m for the Hillside Aquifer. A linear, point-wise kriging

 DOI 10.1007/s10040-009-0504-5

method was used to convert point wise groundwater head data to equipotential lines over the model domain. The equipotential lines converge in the western part of the study area and diverge in the eastern part. Their distribution resembles the topographic contours probably because the hydraulic conductivity of the Coastal Aquifer extending at lower elevations is much greater than the Hillside Aquifer lying over the mountain slope.

Because of the limited number of pumping and laboratory tests, data on the spatial distribution of hydraulic conductivity and effective porosity within the model domain are scarce, particularly in the northeastern and in the north of the western part of the study area where the Hillside Aquifer spreads (see Fig. 1). However, lithologic well logs are available for many of the operating and exploration wells. Therefore, a block kriging technique was applied to estimate the distribution of hydraulic conductivity and effective porosity on the basis of the lithologic descriptions of 194 well logs (Hatipoglu and Bayari 2005a). For this purpose, the GSLIB gamv and kt3d geostatistical software packages (Deutsch and Journal 1998) were used for variogram model and kriging estimation of the spatial distribution of these parameters. The mean hydraulic conductivities were found to be 9 m/day for the Hillside Aquifer and 45 m/day for the Coastal Aquifer. The effective porosities estimated for the Hillside and Coastal Aquifers are 0.07 and 0.09, respectively. The vertical hydraulic conductivity distribution was assumed to obey the vertical to horizontal hydraulic conductivity ratio (Kz/Kh) of 0.1 (e.g., Todd 1980).

An average discharge rate of 79×10^3 m^3/day was attributed to 59 operating wells based on the information gathered from the General Directorate of State Hydraulic Works (DSI, unpublished data, 2002). However, field observations reveal that the number of operating wells may outnumber this value because of the private wells, which have not been registered by the DSI. While the exact magnitude of total abstraction by wells in the study area is difficult to know, the uncertainty associated with this parameter seems to have a negligible effect on the model because of its low magnitude compared to other water budget components (see below).

The model was run at steady state because temporal data required for transient simulation (e.g. abstraction rates and operation periods of the pumping wells) were not available. The head measurements repeated in 29 wells in 2002 resulted in an average head change of 0.21 m compared to the values used in the model. Similarly, the levels in streams and drains have also been found to be stable during the several years that bracket the modeling period. These observations have been regarded as the indicators of a quasi steady-state flow in the aquifer system.

Grid construction

The study area was discretized with a finite-difference grid that was composed of 80 rows and 120 columns with uniform cell dimensions of 500 m by 500 m. The model area is 754.25 km^2, with 3,017 active cells in each layer (Fig. 10). A digital topography map, prepared with MapInfo (1998) software, was used to determine the cell elevations. The model domain was divided into six layers (Fig. 11). The first, second, and third layers were mainly constructed to represent different properties of the Coastal Aquifer. The first layer represents the impermeable part in the southeastern coastal plain, the second layer was constructed for the drainage canal in the same area, and the third layer was used to represent the deeper part of the Coastal Aquifer. Because the entire flow domain was modeled as a single system, all these layers continue toward the Hillside Aquifer where the properties of this aquifer were attributed to these layers. The fourth, fifth and sixth layers were used to represent solely the Hillside Aquifer. The top elevations of the layers 1, 2, 3, 4, 5 and 6 with respect to the sea level were set to range between 600 m and 0 m, +302 m and –1 m, +3 m and –8 m, +2 m and –340 m, –120 m and –347 m, –240 m and –354 m respectively (see Fig. 11). The first layer was modeled as an unconfined aquifer, and the other layers were modeled as confined-unconfined type. The leakance was calculated automatically by the model considering the local hydraulic conductivity and the geometric properties.

Boundary conditions

The northern boundary of the model, which is formed by the low hilly area of the Taurus Mountains where Neogene rocks belonging to the Hillside Aquifer extend, was defined as a specified head boundary. Similarly, the southern boundary, along which the Coastal Aquifer contacts with the Mediterranean Sea, was defined as a specified head boundary. The Berdan and Karakuz Rivers, located at the eastern and western ends of the model domain, respectively, were represented by river boundary conditions.

A firm knowledge on the hydraulic behavior of the Hillside Aquifer at depths below the bottom of the model domain does not exist. However, a no-flow boundary condition for the model bottom was assumed because of the increasing clay and marl content towards the depths of the Hillside Aquifer. Because the Kh/Kz was selected to be 10 in the Hillside Aquifer, the vertical component of recharge from the Paleozoic carbonates to the bottom of the Hillside Aquifer was assumed negligible. The bottom elevation of the model domain was chosen arbitrarily to be 20 m deeper than the bottom elevation of the Coastal Aquifer along the coastline (see Fig. 11). The internal cells were defined as variable head cells. Along the northern boundary, the spatial groundwater level values, as estimated by geostatistical methods, were assigned to the nearest specified head cells. An elevation of 600 m, roughly corresponding to the elevation of the northern model boundary, was arbitrarily assigned to all active cells as the initial groundwater level. Water levels in rivers were assumed 1 m higher than the riverbed elevations, which

 DOI 10.1007/s10040-009-0504-5

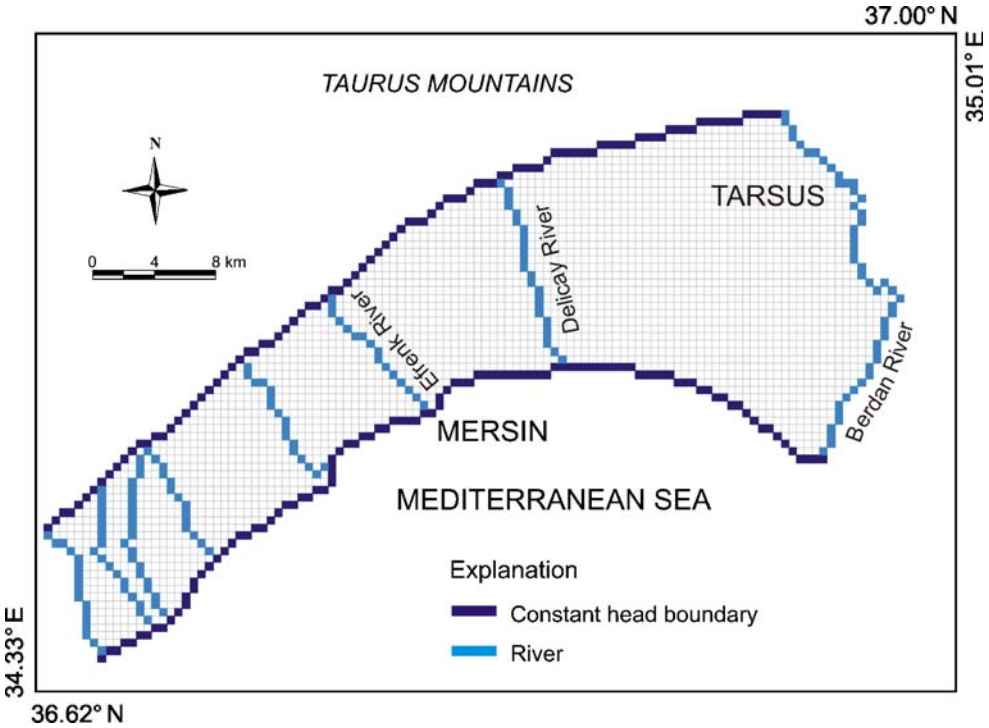

Fig. 10 Finite-difference grid for the upper layer

were determined from the topographic maps. The drainage canal, located at the eastern coastal plain, forms the main drain in the study area and was simulated with the drain package. The data on drain geometry and the thickness of the bed material were taken from DSI (DSI, unpublished data 1990). The hydraulic conductivity of material surrounding the drain was arranged during the calibration process and was found to range between 1.3 m/day and 27 m/day. These values appear to be in agreement with the grain size distribution of the alluvium along the drain.

The groundwater flow pattern is affected by the higher total dissolved solids (TDS) concentration of the seawater in the coastal areas. Equivalent freshwater heads were calculated to account for the density difference between freshwater and seawater and used for the specified constant head cells located along the Mediterranean coast, on the south boundary of the model area. Equivalent freshwater heads were computed by using Eq. 1 (Guo and Langevin 2002):

$$h_f = \frac{\rho}{\rho_f} h - \frac{\rho - \rho_f}{\rho_f} Z \tag{1}$$

where:

h_f is equivalent freshwater head (L);
h is head (L);
ρ_f is density of freshwater (ML^{-3});
ρ is the density of saline aquifer water (ML^{-3}); and
Z is elevation of point N above datum (L)

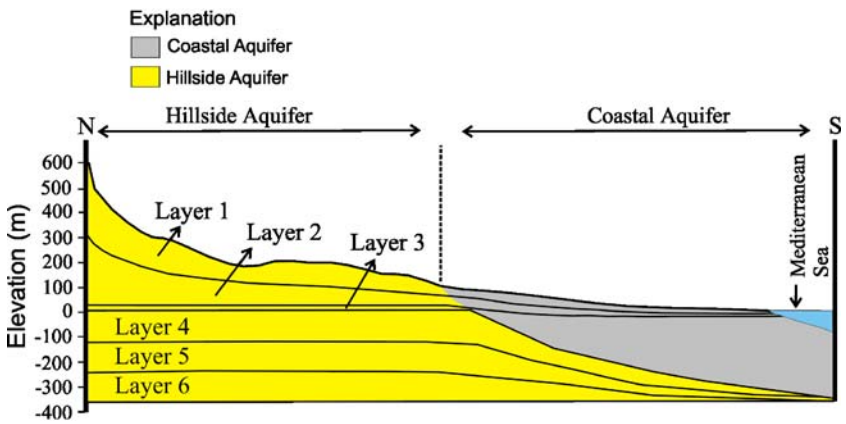

Fig. 11 Schematic view of vertical grid discretization

 DOI 10.1007/s10040-009-0504-5

Steady-state calibration

During the initial stages of model calibration, it was observed that the major deviations between the observed and simulated heads exist in the northwestern and in the northeastern parts of the flow domain. These areas correspond to the regions in the Hillside Aquifer where both the hydraulic conductivity and the observed head distributions were estimated on the basis of spatially limited data because of the sparse distribution of wells. To improve the match between observed and simulated heads in these zones, hydraulic conductivity values were changed zone by zone only in this part of the Hillside Aquifer that extends along the mountain flank. However, the hydraulic conductivities along the river beds within the western part of Hillside Aquifer were manually set to obtain a reasonable fit between the observed and simulated heads. In other parts of the flow domain (i.e. Coastal Aquifer), the hydraulic conductivity distribution obtained from initial geostatistical estimation was not changed because of the reasonably good fit obtained between the observed and simulated heads. However, at the eastern part, hydraulic conductivities along the bed of Berdan River were required to change manually in order to obtain a good fit between observed and simulated heads. At the final stage of calibration, horizontal hydraulic conductivities in the Hillside Aquifer were about half of the initial geostatistical estimates (Fig. 12). The calibrated model revealed residual heads, which are normally distributed with a standard deviation of 5.95 m. About 66% of the residual heads is between ± 0 and 5 m asl (Fig. 13). The zones where the fit between observed and simulated heads is weaker comprise of the areas around riverbeds in the western part and the area along the eastern boundary, which is formed by Berdan River. Because both zones suffer from lack of adequate field data, the observed discrepancy between the observed and simulated head fields may be a result of unrealistic representation of the field conditions by the geostatistical software. Moreover, some of the head measurements may include transient effects so that, while the wells were not operating at the time of head measurement, their water level may not have returned to the local water table particularly at wells surrounded by low hydraulic conductivity zones.

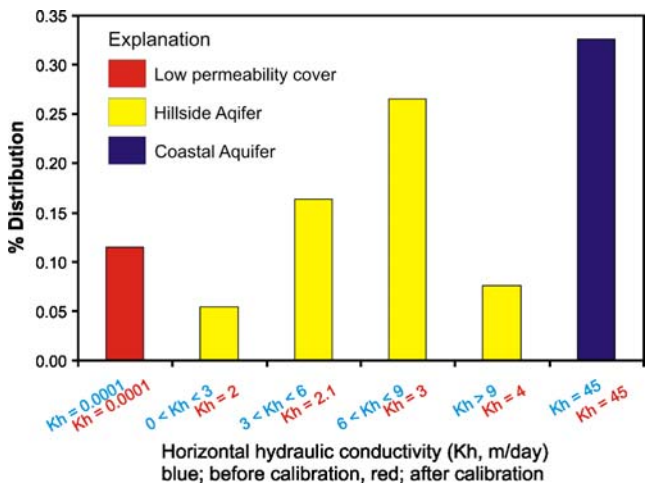

Fig. 12 Distribution of hydraulic conductivities in upper layer before and after the calibration

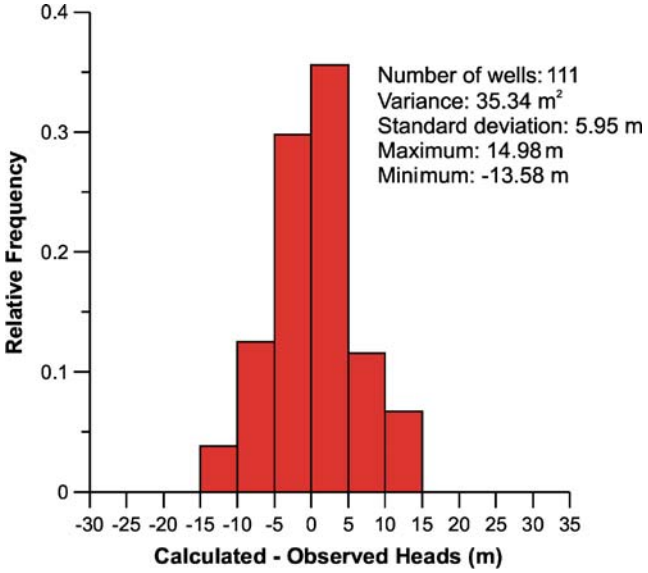

Fig. 13 Histogram of residual heads

Water budget

As expected from a steady-state model, the water budget shows a good balance between inflows and outflows (Table 3). The total steady-state recharge to and discharge from the calibrated model is 4.05×10^6 m^3/day. As inferred by the conceptual model, groundwater inflow from the Taurus Mountains supplies most of the recharge to the aquifer system (3.66×10^6 m^3/day or 90% of the total recharge). The drainage basin extending toward the Taurus Mountains from the Hillside and Coastal Aquifer system is about 3,500 km^2 and is occupied mostly by karstic carbonate rocks possessing very high infiltration capacity. In this area, the net mean annual recharge from precipitation (i.e., 700 mm) corresponds to a mean annual groundwater recharge of 2.45×10^9 m^3 about 30% of which sustains the streams draining the karst aquifer. Therefore, the remaining subsurface discharge of the karst aquifer may be assumed about 1.72×10^9 m^3/year. While this amount is about 28% above the karstic recharge anticipated by the numerical flow model (i.e., 3.66×10^6 m^3/day or 1.34×10^9 m^3/year), the difference

Table 3 Water budget of the numerical groundwater flow model

Recharge	m^3/day	m^3/year	m/day	m/year	% weight
Constant head	3.66E+06	1.34E+09	4.86E-03	1.77	90.39
River	3.29E+05	1.20E+08	4.36E-04	0.16	8.12
Recharge	6.03E+04	2.20E+07	7.99E-05	0.03	1.49
Total	4.05E+06	1.48E+09	5.37E-03	1.96	100.00
Discharge	m^3/day	m^3/year	m/day	m/year	% weight
Constant head	3.17E+06	1.16E+09	4.20E-03	1.53	78.18
River	5.71E+05	2.09E+08	7.58E-04	0.28	14.10
Wells	7.90E+04	2.88E+07	1.05E-04	0.04	1.95
Drains	2.34E+05	8.52E+07	3.10E-04	0.11	5.76
Total	4.05E+06	1.48E+09	5.37E-03	1.96	100.00

DOI 10.1007/s10040-009-0504-5

may be attributed to the uncertainties associated with the exact amount of bulk and effective precipitation rates in the Taurus Mountains. For example, if the real effective recharge is 10% lower than the value attributed above, the karst groundwater recharge into the model domain would be 1.54×10^9 m^3/year. In this case, the above difference reduces to 15%. It is also possible that part of the recharge to the mountainous karst aquifer may reach the sea by flowing under the model domain. Thus, considering uncertainties associated with the spatial extent of the karst aquifer and its discharge to streams, the model-predicted recharge from the karst aquifer appears to be in agreement with what is inferred from the hydrologic budget calculations. Moreover, in agreement with field observations, the contribution of precipitation over the model domain is very small and corresponds roughly to 1.5% of the total input. It appears that the contribution rate of rivers to the recharge of the aquifer (8.1%) is about 5 times greater than the contribution by effective precipitation. This situation is in agreement with the fact that many of the rivers at their upper reaches feed the aquifer as indicated by observed or simulated head distribution (see Fig. 14).

The water budget shows that most of the discharge (78%) from the aquifer system occurs along the sea coast. This situation is in agreement with the fact that little seawater intrusion is observed along the coastline where many of the abstraction wells are located. It appears that the strong groundwater outflow towards the sea prevents widespread seawater intrusion. The second important source of groundwater outflow appears to be the discharge into rivers (14%). This is in agreement with the sustained flow in rivers during the long dry period. The water budget infers 3.8 m^3/s of mean annual river recharge to the aquifer and 6.6 m^3/s of mean annual aquifer recharge to the rivers. Therefore, the net mean annual recharge by the aquifer system is 2.8 m^3/s. Unfortunately, this value can not be validated quantitatively because the rivers draining the aquifer do not have long-term records. The water budget also shows that the discharge by the wells (2%) and drain system (5.8%) is negligible compared to recharge to rivers and discharge into the sea. Therefore, data input errors associated with the wells and drain system appear to have a tolerable effect on the model results. Eventually, the most striking result in the water budget is the obvious role of recharge by karst groundwater supplied from the Taurus Mountains. While the role of a mountain range in recharge of the neighboring coastal aquifer system is already evident on theoretical grounds, determination of the magnitude of this flux is still critical for proper aquifer management.

Hydraulic travel times

As a part of the characterization of the groundwater flow system in the Hillside and Coastal Aquifer system, hydraulic travel times of groundwater along three different sections of the flow domain were calculated by using the PMPATH modeling package (Chiang and Kinzelbach 2001). The PMPATH package utilizes the groundwater velocity field established by the calibrated flow model to calculate the time of travel of a particle along the flow line that extends between the selected upgradient and downgradient sites. For this purpose, travel times were calculated along the linear sections selected in the eastern, central and western parts of the aquifer system (see Fig. 14). The hydraulic travel times, as determined by the PMPATH routine varies from 106 years at the eastern section (18 km) to 153 years in the middle section (9 km) and to 14 years at the western section (8 km; Fig. 14). These hydraulic travel times (i.e. ages) seem to be in agreement with the tritium-based travel times of ground-

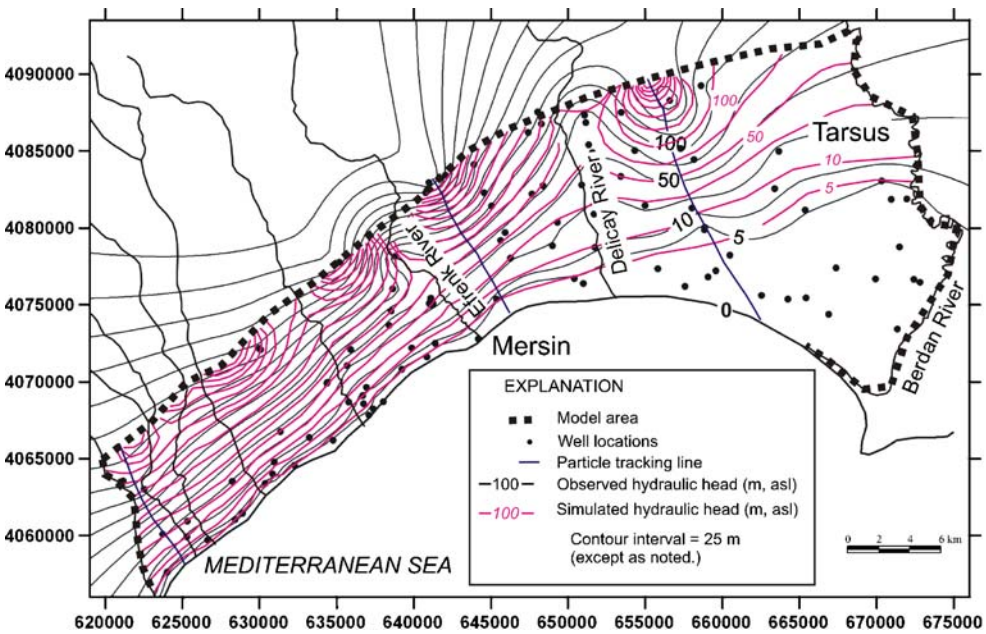

Fig. 14 Distribution of observed and simulated hydraulic heads

 DOI 10.1007/s10040-009-0504-5

water in respective regions (see previous section Environmental isotopes). However, tritium-based travel times are based on a piston flow model, which assumes no mixing among subsequent recharge events. This assumption rarely validates itself in natural flow systems. The travel of the tritium isotope in groundwater flow systems usually follows an exponential flow model that assumes complete mixing between the subsequent recharge waters (e.g. Ozyurt and Bayari 2003, 2005). Consequently, the realistic tritium-based travel times could be much longer than those inferred from the piston flow-model assumption. Therefore, the quantitative resemblance between the tritium-based and hydraulic travel times should be regarded as incidental. However, the travel times inferred by both methods are correlated so that the ages obtained from both methods gets younger from eastern part of the study area to the western part. This situation may be regarded to be another validation of the conceptual model.

Conclusions and outlook

The Hillside and Coastal Aquifer system in the Mersin-Tarsus area of southern Turkey is an important water resource in a region where the demand for groundwater is expected to increase steadily. A conceptual model based on combined analysis of hydrochemical and environmental isotopic data reveals that the present aquifer system is mainly fed by the karst aquifer that extends in large areas over the Taurus Mountains located to the north. Accordingly, the steady-state numerical groundwater flow model applied in this study validates this conceptual perspective and suggests that about 90% of recharge to the aquifer is supplied by the mountainous karst aquifer. Despite the vast distribution of groundwater abstraction wells along the coastal zone, the negligible seawater intrusion appears to be a result of strong seaward outflow that is maintained by this recharge. Under present conditions, the aquifer also seems to be a critical source in maintaining the flow of the neighboring rivers.

The results of this study imply an aquifer system that has not been disturbed considerably. Yet, several factors need to be considered by local water-policy makers in planning the future water use. The amount of karst groundwater recharge from the Taurus Mountains is much greater than the current groundwater discharge from wells, rivers and the drain system. Therefore, increasing the current groundwater abstraction rate by wells up to several orders of magnitude does not result in a negative water balance in the aquifer. However, at its near-pristine state, the current groundwater system functions almost naturally and distributes the recharge from various sources to discharges in the form of various sinks that include well abstraction, recharge to rivers and drain systems and into the sea. Consequently, allocating more groundwater for well abstraction in the future will eventually decrease the share of other sink components. Such a practice, depending on its locality, may lead to a depleted river flow or seawater intrusion. Therefore, before establishing a new water use policy, its environmental consequences must be considered carefully. To prevent these potential problems, all parameters to be required in future reassessment of the conceptual and numerical models have to be collected systematically. This requires establishment of a well-planned and well-maintained monitoring system that could produce more systematic data to be used in future assessment studies. In this context, monitoring of the hydrologic regime in the mountainous part bears special importance, as this area is the source of major recharge. Because the current changes in global climate may eventually affect the recharge regime in the mountain zone, anticipation of these changes will probably be much more important than the management of water use in the aquifer system.

Acknowledgements The authors express thanks to E. Oncel, F. Muslu and N. Ozyurt for their generous support with the analyses at the Water Chemistry and Environmental Tritium Laboratories of Hacettepe University. Funding for the stable isotope analyses was provided by various grants from the Scientific and Technical Research Council of Turkey (TUBITAK) and research funds of Hacettepe University and the University of Mersin.

References

APHA, AWWA, WPCF (1989) Standard methods for the examination of water and wastewater. APHA, Washington DC

Appelo CAJ, Postma D (2005) Geochemistry, groundwater and pollution, 2nd edn. Balkema, Amsterdam

Bayari CS (1991) Karst hydrogeological investigation of the Lower Zamanti Basin (Aladaglar) (in Turkish). PhD Thesis, Hacettepe University, Institute of Graduate Studies, Turkey

Bayari CS (2008) Recovery of fresh water discharges along turkish coast: patara-tekirova pilot project (TUBİTAK CAYDAG-103Y025) (in Turkish). Final Report, TUBITAK, Ankara, 179 pp,

Bayari CS, Kurttas T (2002) Coastal and submarine karstic discharges in the Gökova Bay, SW Turkey. Q J Eng Geol Hydrogeol 35:381–390

Boronina A, Renard P, Balderer W, Christodoulides A (2003) Groundwater resources in the Kouris catchment (Cyprus): data analysis and numerical modeling. J Hydrol 271:130–149

Chiang WH, Kinzelbach W (2001) 3D-groundwater modeling with PMWIN: a simulation system for modeling groundwater flow and pollution. Springer, Berlin

Craig H (1961) Isotopic variations in meteoric waters. Science 133:1702–1703

Demirel Z (2004) The history and evaluation of saltwater intrusion into a coastal aquifer in Mersin Turkey. J Environ Manage 70 (3):275–282

Deutsch CV, Journal AG (1998) Geostatistical software library and users guide. Oxford University Press, New York

Fetter CW (2007) The concept of safe groundwater yield in coastal aquifers. J Am Water Resour Assoc 8(6):1173–1176

Gat JR, Carmi I (1970) Evolution of the isotopic composition of fresh water occurrences in Israel and the northern Jordan Rift Valley. J Hydrol 16:177

Governorship of Mersin (2006) Mersin′s environment report. Department of Environment and Forestry, Governorship of Mersin, Mersin, Turkey, 296 pp

Gunay G, Elkhatib H (1988) Hydrogeological investigation of the karst submarine springs on the Mediterranean coast of Turkey by means of remote sensing technique. Proceedings of the Symposium on Karst Hydrogeology and Karst Environment Protection, IAH 21st Congress, Guilin, China, 10-15 October 1988, pp 474-483

 DOI 10.1007/s10040-009-0504-5

Guo W, Langevin CD (2002) User′s guide to SEAWAT: a computer program for simulation of three-dimensional variable-density groundwater flow. In: Techniques of water-resources investigations. Book 6, Chapter A7, US Geological Survey, Reston, VA

Harbaugh AW, McDonald MG (1996), User′s documentation for MODFLOW-96: an update to the U.S. Geological Survey modular finite-difference ground-water flow model, US Geol Surv Open-File Rep 96-485

Hatipoglu Z (2004) Hydrogeochemistry of Mersin-Tarsus coastal aquifer (in Turkish with English abstract). PhD Thesis, Hacettepe University, Institute of Pure and Applied Sciences, Turkey, 142 pp

Hatipoglu Z, Bayari CS (2005a) Hydrogeochemistry of Mersin-Tarsus hillside and coastal aquifers (in Turkish with English abstract). Turkiye Jeol Bul 48(2):57–72

Hatipoglu Z, Bayari CS (2005b) Three dimensional kriging analysis of hydraulic conductivity and effective porosity: an example from Mersin-Tarsus hillside and Coastal Aquifers (in Turkish with English abstract). Jeoloji Mühendisligi Dergisi 29(2):1–9

IAEA (1992) Statistical treatment of data on environmental isotopes in precipitation. Technical reports series no. 331, IAEA, Vienna

Idrysy H, Smedt F (2006) Modelling groundwater flow of the Trifa aquifer, Morocco. Hydrogeol J 14:1265–1276

Jiao JJ, Leung CM, Ding GP (2008) Change of the groundwater system, from 1888 to present, in a highly-urbanized coastal area in Hong Kong, China. Hydrogeol J 16(8):1527–1539

MapInfo (1998) MapInfo professional 5.5 software package. MapInfo, New York

McDonalds MG, Harbaugh AW (1988) A modular three-dimensional finite-difference ground-water flow model. Techniques of Water-Resources Investigations, Book 6, chapter A1, US Geological Survey, Reston, VA

Monteith JL (1965) Evaporation and environment, In: Proceedings of the 19th Symposium of the Society for Experimental Biology. Cambridge University Press, New York, pp 205–233

Ozyurt NN (2005) Investigation of the residence time distribution in the Aladag (Kayseri-Adana, Turkey) karstic aquifer (in Turkish). PhD Thesis, Hacettepe University, Institute of Graduate Studies, Turkey

Ozyurt NN, Bayari CS (2003) LUMPED: a visual basic code of lumped parameter models for mean residence time analysis in groundwater systems. Comput Geosci-UK 29(1):79–90

Ozyurt NN, Bayari CS (2005) LUMPED unsteady: a visual basic code of unsteady-state lumped-parameter models for residence time distribution analyses of groundwater systems. Comput Geosci-UK 31(3):329–341

Ozyurt N, Bayari S (2007) Temporal variation of chemical and isotopic signals in major discharges of an alpine karst aquifer in Turkey: implications with respect to response of karst aquifers to recharge. Hydrogeol J 16(2):297–309. doi:10.1007/s10040-007-0217-6

Palma HC, Bentley LR (2007) A regional-scale groundwater flow model for the Leon-Chinandega aquifer, Nicaragua. Hydrogeol J 15:1457–1472

Senol M, Sahin S, Duman TY (1998) The geological investigation of the Mersin region (in Turkish). General Directorate of Mineral Research and Exploration of Turkey, Ankara

Todd DK (1980) Groundwater hydrology. Wiley, New York

Turc L (1954) Le bilan d′eau des sols; relations entreles precipitations, I′ evaporation et I′ecoulement [The water assessment of the grounds; relations between precipitations, evaporation and flow]. La Hauille Blanche L′union Hydrotechnigue de France, Paris

Turkmen G (1978) Mersin-Berdan and Efrenk plains hydrogeological investigation report (in Turkish). General Directorate of Rural Services, Ankara

Unterwerger MP, Lucas LL (2000) Calibration of the national institute of standards and technology tritiated-water standards. Appl Radiat Isotopes 52:527–531

Vandenbohede A, Houtte EV, Lebbe L (2009) Sustainable groundwater extraction in coastal areas: a Belgian example. Environ Geol 57(4):735–747. doi:10.1007/s00254-008-1351-8